Phase Chemistry and Precipitation Reactions in Maraging Steels: Part I. Introduction and Study of Co-Containing C-300 Steel

W. SHA, A. CEREZO, and G.D.W. SMITH

This article introduces a series of studies of phase transformations in maraging steels. Atom-probe field-ion microscopy (APFIM) was the main research technique employed. Hardness measurements, transmission electron microscopy (TEM), and thermochemical calculations were also used. The composition and morphology of precipitates in the commercial-grade C-300 steel were compared for different aging times at 510 °C to investigate the aging sequence. Both Ni_3Ti and Fe_7Mo_6 were found to contribute to age hardening. The decomposition starts with the formation of small Mo-enriched Ni_3Ti particles at very short aging times. The Fe_7Mo_6 phase forms at a later stage of aging. The matrix concentrations of both Ti and Mo were measured and were found to be low after standard aging conditions. The observation of the Fe_7Mo_6 μ phase is supported by thermochemical calculations. Austenite reversion has been found at the aging temperature, and its composition approaches the predicted equilibrium composition after 8 hours of aging.

I. INTRODUCTION

MARAGING steels are a special class of ultrahigh-strength martensitic steels which are age-hardened by the precipitation of intermetallic compounds.[1,2,3] Since their initial development in the late 1950s, maraging steels have found a wide range of applications. A large amount of research work was carried out on the physical metallurgy of these alloys in the early years after their invention. This interest has been renewed in the last decade, prompted by the sharp drop in the availability of cobalt in the late 1970s. Although much work has focused on what happens in hardening reactions during aging, the exact nature of the precipitation process is still, to a large extent, unknown. This is due to the high density of extremely fine precipitates embedded in the martensite matrix (of the order of 10 nm in size and 10^{23} m^{-3} in density[4]). Generally, it is believed that Ni_3X (X = Ti, Mo, V, W) type phases form at the earlier aging stage,[1-3,5,6] while the more stable Fe-Y (Y = Mo, W) type phases[1-3,7,8] appear after longer aging times. However, different results have been reported even on the same material and after the same heat treatment. The similarity of diffraction patterns from the different possible precipitate phases makes their identification difficult using transmission electron microscopy (TEM) techniques.

Vasudevan *et al.* studied the crystallography, structure, and composition of the maraging precipitates in two commercial steels, VASCOMAX C-250 and T-250,* using analytical electron microscopy and computer-simulated electron diffraction patterns.[9,10] The kinetics of precipitation were studied by electrical resistivity and microhardness measurements. The results indicate that precipitate nucleation occurs on dislocations and that growth proceeds by a mechanism in which the dislocations serve as collector lines for solute from the matrix. The strengthening of the Co-free, higher Ti T-250 steel is caused by a refined distribution of Ni_3Ti precipitates. High strength is maintained at longer aging times due to the combined effect of the high resistance of these precipitates to coarsening and the small volume fraction of reverted austenite. In the case of Co-containing, lower Ti, C-250 steel, these authors report the combined presence of Ni_3Ti precipitates (initially) and Fe_2Mo (at longer aging). Loss of strength at longer times is partly associated with overaging but is mainly due to the larger volume fraction of reverted austenite. The resistance to austenite reversion depends on the relative Ni content of the martensite matrix which, in turn, is affected by the precipitation of Ni_3Ti.

Atom-probe field-ion microscopy (APFIM) has proved capable of revealing the distribution of small precipitates and accurately analyzing their compositions on an atomic scale.[11] There have been a few APFIM studies of maraging-type steels, mostly model alloys, which revealed atomic-scale features, such as grain boundary Mo segregation.[5,6,12,13] However, quantitative microanalysis of commercial steels has not been available, due to the restricted mass resolution of the instruments used. We have the high mass resolution, energy-compensated, Oxford FIM100 system, together with the newly developed

*VASCOMAX C-250 and T-250 are trademarks of Teledyne Vasco (formerly Vanadium Alloy Steel Company), Latrobe, PA.

W. SHA, formerly Graduate Student with the Department of Materials, Oxford University, is with the Department of Materials Science and Metallurgy, Cambridge University, Cambridge CB2 3QZ, United Kingdom. A. CEREZO, Royal Society Research Fellow, and G.D.W. SMITH, University Lecturer, are with the Department of Materials, University of Oxford, Oxford OX1 3PH, United Kingdom.

Manuscript submitted July 31, 1992.

position-sensitive atom probe (POSAP),[14] to examine complex commercial grades, such as VASCOMAX C-300*. Preliminary results have already been reported.[14–19] The present series of articles represent the extension and completion of this work.

*VASCOMAX C-300 is a trademark of Teledyne Vasco (formerly Vanadium Alloy Steel Company), Latrobe, PA.

The commercial alloy, C-300 (for composition, see Table I*), was chosen partly because it has been the subject of field-emission scanning transmission electron microscopy (STEM) investigations by Vanderwalker[20,21] and small-angle scattering studies by Servant *et al.*[22] The aging temperature in this work was chosen to be 510 °C. This is partly because of practical toughness considerations. Three-hundred ksi grade steels generally have a lower toughness than lower strength grades (250 and 200 ksi). However, by raising the aging temperature from 482 °C (the more usual industrial treatment temperature) to 510 °C, the toughness can be greatly improved.[23]

*All compositions quoted in this series of articles are given in atomic percent.

In the following sections, after a statement of experimental approach, conventional hardness measurements and electron microscopy studies are described briefly. The APFIM results for each aging stage follow. After presenting these experimental data, thermochemical calculations are used to aid the interpretation of results.

II. EXPERIMENTAL

The C-300 steel was originally made by the Vanadium Alloy Steel Company, Latrobe, PA. Samples, in the form of 10-mm-thick plate, were supplied courtesy of Dr. D.M. Vanderwalker of the United States Army Materials Technology Laboratory, Watertown, MA. The homogeneity of the as-supplied samples was checked by electron probe microanalysis using a Cameca Camebax microanalyzer. The results show a good homogeneity, with the composition variation for major constituents within the analysis error (±0.2 pct).

Samples for hardness measurements and TEM examination were prepared with dimensions of about 1 × 10 × 30 mm. Specimens were sealed in silica tubes with vacuum $<10^{-5}$ mbar, annealed at 816 °C for 2 hours, and water quenched. They were subsequently aged at 510 °C for different times. Water quenching was used after aging treatments.

The hardness measurements were made on a Vickers Pyramid hardness testing machine, with a 294 N load. Each data point was averaged from eight measurements.

Transmission electron microscopy thin foil specimens were made by electropolishing using a solution consisting of 5 pct perchloric acid in acetic acid with a voltage of 35 V, a current of 40 to 50 mA, and a temperature of ≈0 °C. The TEM studies were carried out using a PHILIPS* EM301 electron microscope.

*PHILIPS is a trademark of Philips Electronic Instruments Corporation, Mahwah, NJ.

For APFIM studies, small bars with dimensions of approximately 0.7 × 0.7 × 10 mm were heat-treated in vacuum. They were then necked by electrolytic polishing in a layer of 25 pct perchloric acid floated on carbon tetrachloride at a temperature of 0 °C to 5 °C and a polishing voltage of approximately 20 V. This first stage lasted 5 to 10 minutes. The next stage was to reduce the neck width by slow polishing in 2 pct perchloric acid in 2-butoxyethanol at room temperature and with 20 V applied, until the weight of the lower section caused it to fracture. It was found that more stable tips were produced if a subsequent micropolishing technique was used. In this process, a new neck is formed behind the initial specimen tip by polishing in a small drop of 2 pct perchloric acid in 2-butoxyethanol at room temperature, with a 10 to 20 V polishing voltage. The majority of specimens used in this work were made using this technique.

The FIM observations were made with neon imaging gas. The usual imaging temperature was 65 K, although in order to obtain adequate contrast from the very smallest precipitates, a higher temperature was needed (≈95 K). Atom-probe analysis was usually conducted at a specimen temperature of 65 K and with a pulse fraction of 20 pct, in order to ensure maximum quantitative accuracy, by eliminating any preferential field evaporation effects.[11] Figure 1(a) shows a FIM100 AP mass spectrum obtained from a molybdenum-rich precipitate in a specimen aged for 30 minutes at 510 °C. There is no difficulty in resolving all of the elements in the alloy by the energy-compensated atom probe, except for the peak overlaps of $^{58}Fe^{2+}$ and $^{58}Ni^{2+}$ and $^{64}Ni^{2+}$ and $^{96}Mo^{3+}$. The ions at these two mass-to-charge ratios were regarded as Fe and Mo, respectively, in the current experiments, which had negligible effect on the overall analysis. The nominal composition and the AP-analyzed composition of as-quenched specimens are in excellent agreement, as shown in Table I. The experimental compositions quoted were all from energy-compensated AP data, unless otherwise indicated.

In conventional atom-probe analysis, the fine-scale compositional variations in the aged material are of primary concern. The simplest way to observe these is to divide the data into samples of appropriate size and observe the variations in the resultant composition profile

Table I. Nominal Composition of the C-300 Maraging Steel and Atom Probe Analyzed Composition of As-Quenched Specimens (Atomic Percent)

Elements*	Ni	Co	Mo	Ti	Al	Si	Fe
Nominal	18.2	8.8	2.9	0.7	0.2	0.2	balance
AP	17.6 ± 0.5	9.1 ± 0.4	3.0 ± 0.2	0.8 ± 0.1	0.2 ± 0.1	0.2 ± 0.1	balance

*The maximum carbon content is 0.1 pct.

(*appropriate* generally implies a sample size showing the composition change of interest, *i.e.*, smaller than the scale of variation of interest but containing sufficient atoms to give reasonable statistics within each sample). In the study of very small particles after short-time aging, a sample size that is the optimum with respect to the sample geometry is preferred. The experimental conditions were set so that the volume of material in each sample was approximately constant and the corresponding cylinder quasi-cubical (height $\approx$ area$^{1/2}$ $\approx$ 1.3 nm). For a more detailed description of data handling techniques, see the monograph by Miller and Smith.[11]

In the more recently developed POSAP, time-of-flight mass spectrometry is combined with position sensing to produce a system which can determine both the chemical identity and initial positions of single atoms field evaporated from the specimen surface.[14] Data are collected from a wider area of the sample, approximately 20 nm in diameter (compared with 2 nm in the conventional AP), and are then analyzed by computer methods to reconstruct the atomic-scale composition of these regions. Because of limited mass resolution, the POSAP is not suitable for quantitative analysis of Fe, Ni, and Co (Figure 1(b)) but is adequate to map the distribution of Ti and Mo.

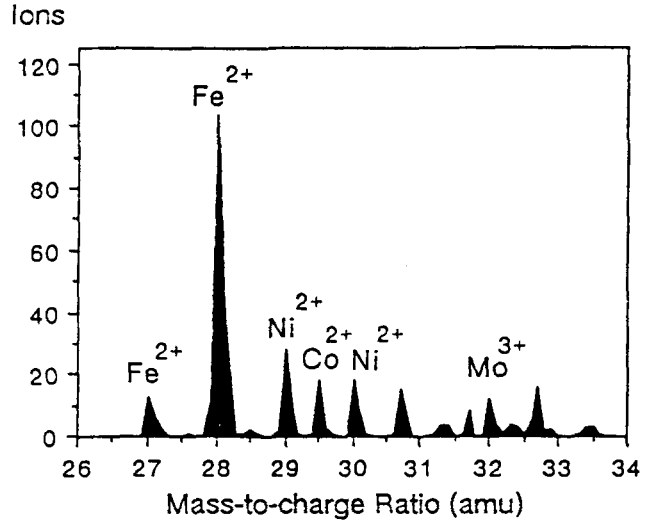

(*a*)

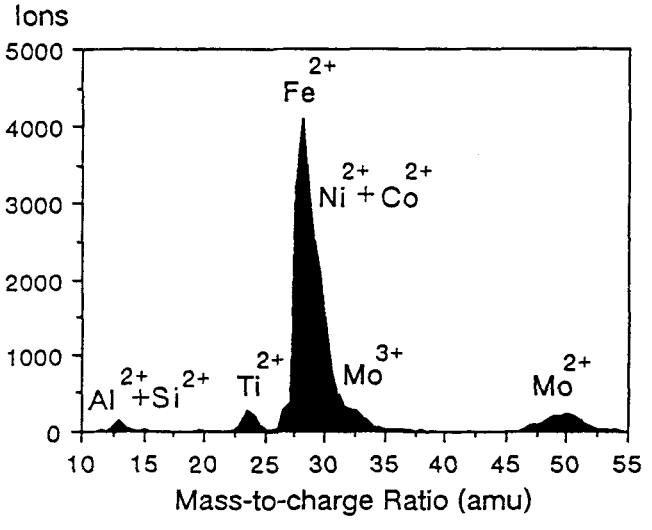

(*b*)

Fig. 1—Mass spectra obtained from regions containing precipitates in the aged C-300 maraging steel by (*a*) energy-compensated VG FIM100 AP and (*b*) the POSAP (amu = atomic mass unit).

III. RESULTS

A. *Hardness Measurements*

For C-300 maraging steel at the aging temperature used in this work (510 °C), the complete hardening curve was not readily available. Vickers hardness measurements were thus made, and the results are shown in Figure 2. The increase of hardness is significant from the very beginning of aging, and peak hardness is reached after 1 hour. The hardness drops to only a limited extent after further aging treatment. Thus, the steel is not very sensitive to under- and overaging as far as aging time at 510 °C is concerned. From the data of Figure 2, we may define three main stages in the aging sequence, as follows:

(1) early stages of precipitation: <30 minutes;
(2) near peak-hardness aging reactions: 30 minutes to 8 hours;
(3) overaging: >8 h.

In order to gain an understanding of the microchemical and microstructural evolution during aging in the maraging steel for all of the stages, the subsequent microstructural study was carried out for aging times in the range from 240 seconds to 128 hours.

B. *TEM Studies*

The TEM/STEM studies of these materials have been carried out by Vanderwalker.[20,21] In the present work, only a short TEM study was made on standard treated and overaged specimens. Figure 3 shows a diffraction pattern obtained from a specimen aged for 4 hours at

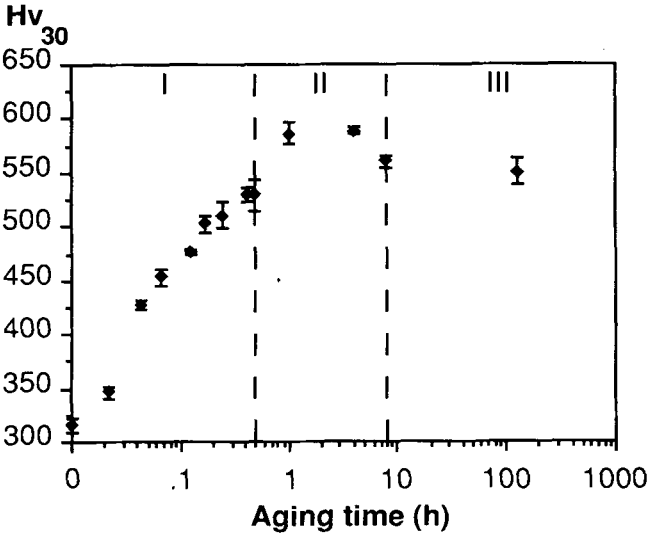

Fig. 2—Hardening curve of the C-300 maraging steel at the aging temperature of 510 °C (Vickers Pyramid hardness, 294N load).

510 °C and corresponding dark-field images. There are obviously very densely distributed precipitates. The precipitates are of the order of 10 nm in size and 10^{23} m^{-3} in density. For the overaged specimen, in addition to the fine precipitates, there are large plates of reverted austenite (Figure 4). The observed shape of the reverted austenite regions agrees with a previous study by Peters.[24] The dense, complicated microstructures of the alloy are hard to analyze by TEM/STEM methods. In particular, quantitative chemical characterization of the phases present is very difficult. Hence, APFIM study is necessary for a fuller understanding of the alloy system.

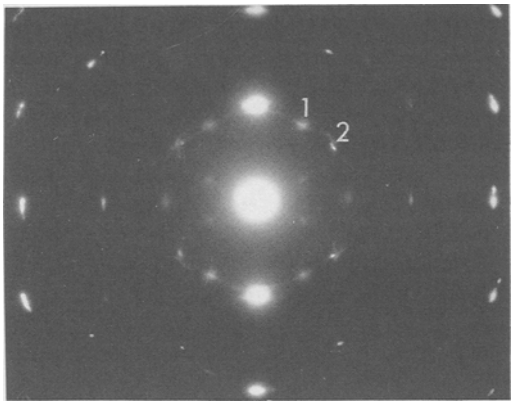

(*a*)

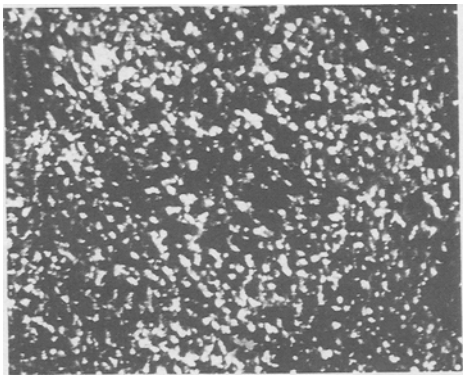

(*b*)

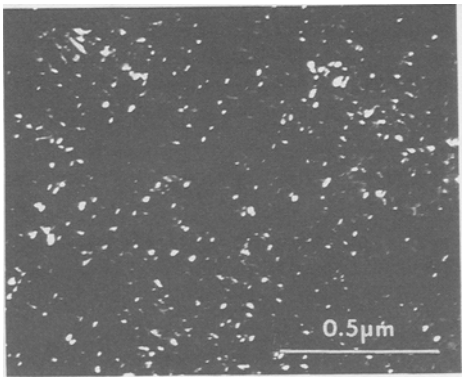

(*c*)

Fig. 3—(*a*) Diffraction pattern obtained from a C-300 maraging steel specimen aged at 510 °C for 4 h, showing diffraction spots from martensite and precipitates; (*b*) dark-field images from spot 1 in (a), showing precipitates; (*c*) dark-field images from spot 2 in (a), showing precipitates.

C. *APFIM Study I—Early Stages of Precipitation*

1. *As-quenched alloy*

The possibility of very small clusters existing in the as-quenched alloy has been examined by FIM and AP microanalysis. Molybdenum atoms image brightly in iron.[25] Therefore, any pronounced clustering effects should be detectable by simple visual observation. There was no observable clustering/segregation effect in FIM images (Figure 5). This kind of observation will not work for Ni and Ti, which give rather little element contrast difference.

POSAP can reveal the clustering of Ti, in addition to Mo. Figure 6 shows a POSAP analysis of an as-quenched specimen, again giving no obvious indication of clustering.

The energy-compensated FIM100 AP is capable of quantitative analysis of all of the elements. Statistical analysis of FIM100 AP data was made which showed

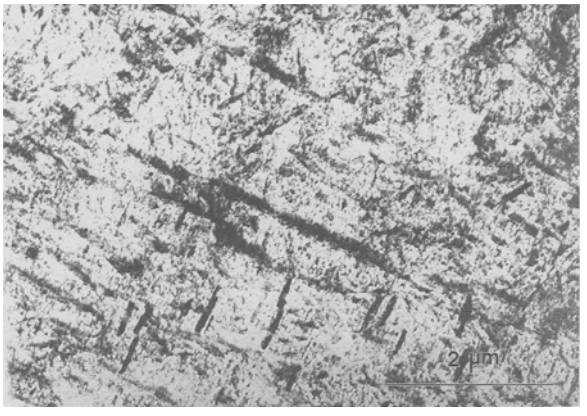

Fig. 4—Bright-field TEM image from an overaged C-300 maraging steel specimen, showing austenite and precipitates. Aging temperature, 510 °C; aging time, 128 h.

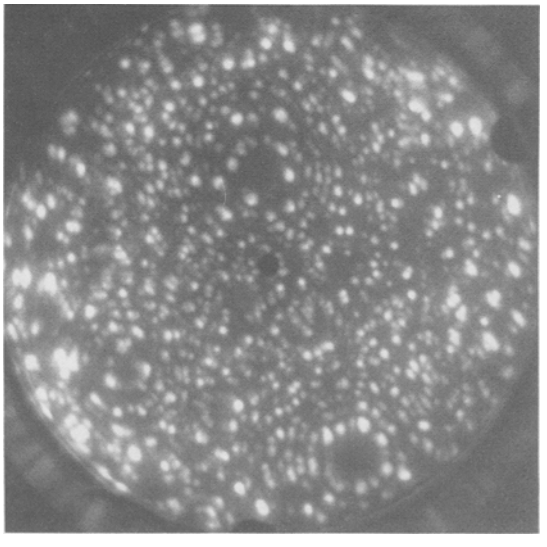

Fig. 5—Field-ion micrograph of an as-quenched C-300 specimen. Distance across the image is ≈60 nm.

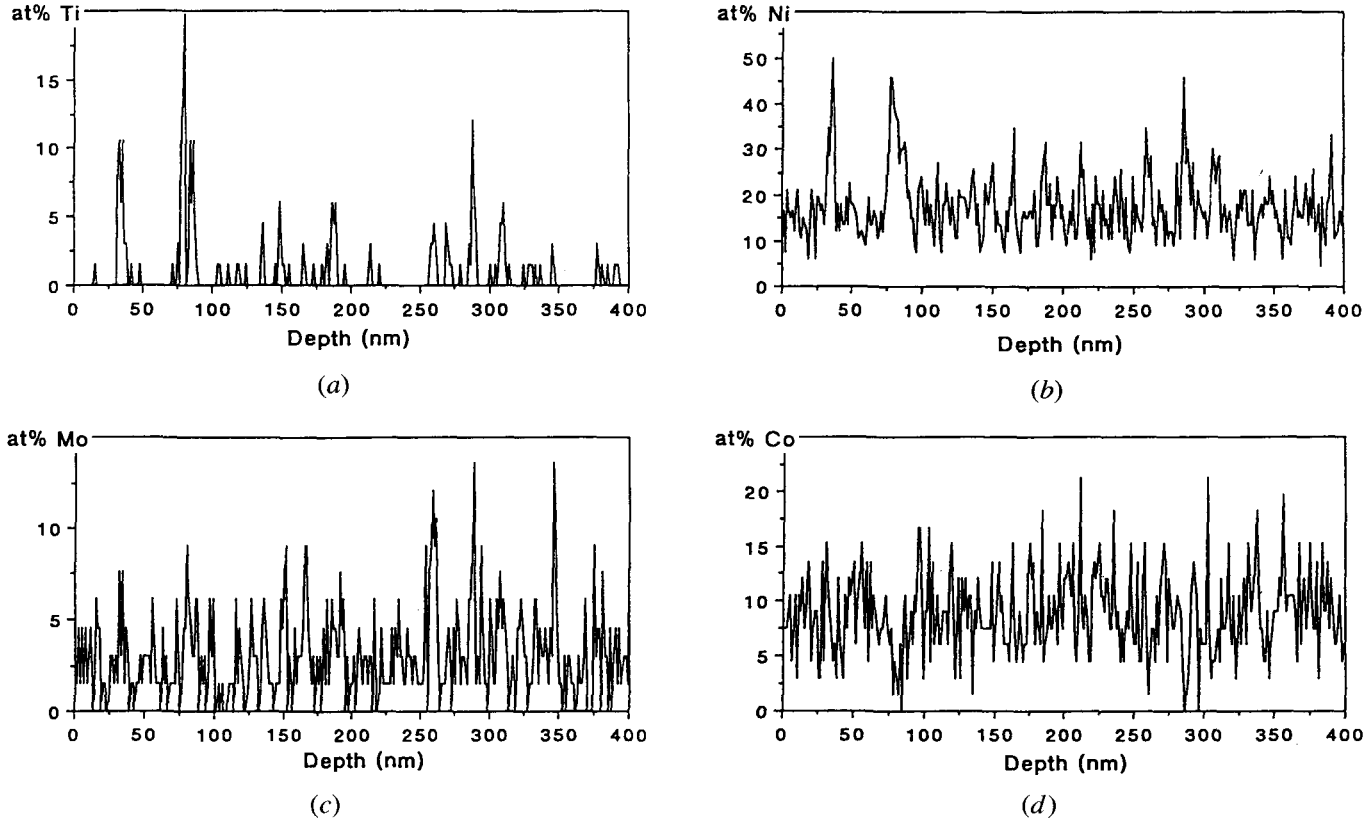

Fig. 8—Composition profile of C-300 maraging steel aged for 460 s at 510 °C. Probing diameter ≈1.4 nm.

Table II. Composition of Particles for Short Aging Times as Determined by FIM100 Atom Probe*

Time (s)	Ni	Ti	Mo	Al	Fe	Co
240	33 ± 9 (23 to 39)	7 ± 4 (4 to 11)	6 ± 2 (4 to 7)	1 ± 1 (0 to 2)	48 ± 11 (39 to 60)	5 ± 4 (2 to 9)
460	27 ± 7 (18 to 46)	8 ± 4 (4 to 17)	5 ± 3 (2 to 11)	<1 (0 to 2)	53 ± 9 (31 to 63)	7 ± 3 (1 to 14)

*Data are given in the form of average compositions ± one standard deviation, together with the maximum and minimum values obtained.

summarizes the compositions of the precipitate regions as calculated from ladder diagrams of FIM100 AP data. Though the compositions of individual particles vary widely, contingency table analysis showed that concentrations of Ni, Mo, and Ti in the particles were correlated (Table III). The observations indicate that the Ni_3Ti precipitate forms first during the aging process in Ti- and Mo-hardened steels, in agreement with previous suggestion by other workers.[9,10] However, the AP results identify a new factor, which is the enrichment of Mo in these particles. There is no obvious separate Mo clustering; instead, Mo and Ti are cosegregated at this early stage of precipitation. The partition of Mo in Ti + Ni-rich particles results in a lowered degree of Mo supersaturation in the matrix. For example, the matrix Mo content is 1.9 ± 0.3 pct for samples aged for 460 seconds, compared to the bulk Mo level of 2.9 pct. One consequence of the rapid kinetics of formation of the Mo-enriched Ni_3Ti precipitates is a reduction in the thermodynamic driving force remaining for the formation of other Mo-rich phases. This will by further discussed in Part IV.[26]

Figure 9 illustrates some POSAP images showing the shape and spatial distribution of the small particles formed after aging. After 460 seconds of aging, the particles are spheroidal, while the particle shape after 240 seconds of aging is not very well defined. There are also regions in 240 second aged specimens where Ti atoms are widely dispersed, indicating that precipitate nucleation may not be complete at this stage. Using the POSAP data, the compositions of the particles can be calculated by selecting the core of Ti-enriched area (1 to 2 nm in size), and these results are given in Table IV. By comparing results in Tables II and IV, it can be seen that the FIM100 AP underestimates the level of Ti in these particles (probably due to probe hole aperture limitations). Therefore, the Ni level in particles measured by FIM100 AP is also very likely lower than the true value, but unfortunately, this element cannot be fully resolved in the POSAP. However, even in the POSAP, the Ti concentration in the particles is measured to be much lower than the stoichiometry of Ni_3Ti in most cases. It seems possible that a gradual enrichment of Ti, as well as other alloying elements, occurs during the formation, growth,

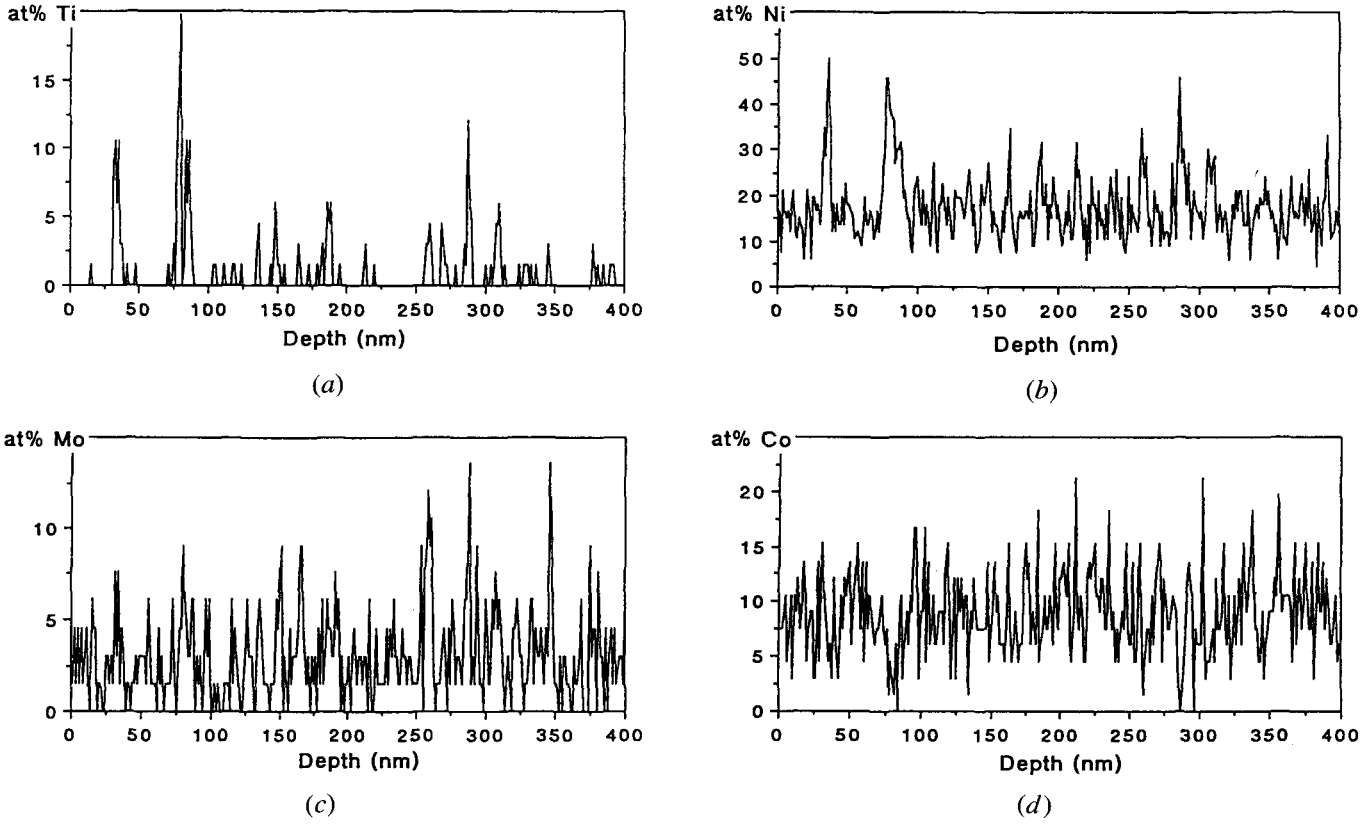

Fig. 8—Composition profile of C-300 maraging steel aged for 460 s at 510 °C. Probing diameter ≈1.4 nm.

Table II. Composition of Particles for Short Aging Times as Determined by FIM100 Atom Probe*

Time (s)	Ni	Ti	Mo	Al	Fe	Co
240	33 ± 9 (23 to 39)	7 ± 4 (4 to 11)	6 ± 2 (4 to 7)	1 ± 1 (0 to 2)	48 ± 11 (39 to 60)	5 ± 4 (2 to 9)
460	27 ± 7 (18 to 46)	8 ± 4 (4 to 17)	5 ± 3 (2 to 11)	<1 (0 to 2)	53 ± 9 (31 to 63)	7 ± 3 (1 to 14)

*Data are given in the form of average compositions ± one standard deviation, together with the maximum and minimum values obtained.

summarizes the compositions of the precipitate regions as calculated from ladder diagrams of FIM100 AP data. Though the compositions of individual particles vary widely, contingency table analysis showed that concentrations of Ni, Mo, and Ti in the particles were correlated (Table III). The observations indicate that the Ni_3Ti precipitate forms first during the aging process in Ti- and Mo-hardened steels, in agreement with previous suggestion by other workers.[9,10] However, the AP results identify a new factor, which is the enrichment of Mo in these particles. There is no obvious separate Mo clustering; instead, Mo and Ti are cosegregated at this early stage of precipitation. The partition of Mo in Ti + Ni-rich particles results in a lowered degree of Mo supersaturation in the matrix. For example, the matrix Mo content is 1.9 ± 0.3 pct for samples aged for 460 seconds, compared to the bulk Mo level of 2.9 pct. One consequence of the rapid kinetics of formation of the Mo-enriched Ni_3Ti precipitates is a reduction in the thermodynamic driving force remaining for the formation of other Mo-rich phases. This will by further discussed in Part IV.[26]

Figure 9 illustrates some POSAP images showing the shape and spatial distribution of the small particles formed after aging. After 460 seconds of aging, the particles are spheroidal, while the particle shape after 240 seconds of aging is not very well defined. There are also regions in 240 second aged specimens where Ti atoms are widely dispersed, indicating that precipitate nucleation may not be complete at this stage. Using the POSAP data, the compositions of the particles can be calculated by selecting the core of Ti-enriched area (1 to 2 nm in size), and these results are given in Table IV. By comparing results in Tables II and IV, it can be seen that the FIM100 AP underestimates the level of Ti in these particles (probably due to probe hole aperture limitations). Therefore, the Ni level in particles measured by FIM100 AP is also very likely lower than the true value, but unfortunately, this element cannot be fully resolved in the POSAP. However, even in the POSAP, the Ti concentration in the particles is measured to be much lower than the stoichiometry of Ni_3Ti in most cases. It seems possible that a gradual enrichment of Ti, as well as other alloying elements, occurs during the formation, growth,

Table III. Contingency Table Analyses for C-300 Maraging Steel Aged for 240 Seconds at 510 °C*

(a) Mo and Ti

	Experimental Observations					Estimates (Random) Values				
Ti/Mo	0 to 1	2	3	4 to 7	Total	0 to 1	2	3	4 to 7	Total
0	24	14	8	4	50	21.0	13.7	8.1	7.3	50
1 to 8	2	3	2	5	12	5.0	3.3	1.9	1.7	12
Total	26	17	10	9	62	26	17	10	9	62

$\chi^2 = 9.9$ with 3 degrees of freedom.

(b) Mo and Ni

	Experimental Observations				Estimates (Random) Values			
Ni/Mo	0 to 1	2	3 to 7	Total	0 to 1	2	3 to 7	Total
6 to 14	21	15	9	45	18.9	12.3	13.8	45
15 to 32	5	2	10	17	7.1	4.7	5.2	17
Total	26	17	19	62	26	17	19	62

$\chi^2 = 9.0$ with 2 degrees of freedom.

*Frequency of (a) Mo and Ti and (b) Mo and Ni in 65-atom blocks. Cosegregation is indicated between Mo and Ti and between Mo and Ni at the 5 pct significance level.

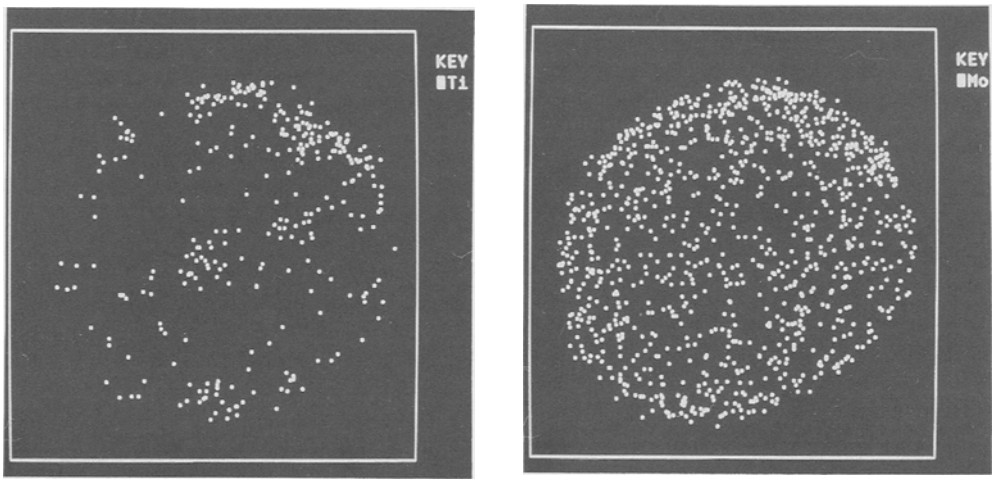

(*a*)

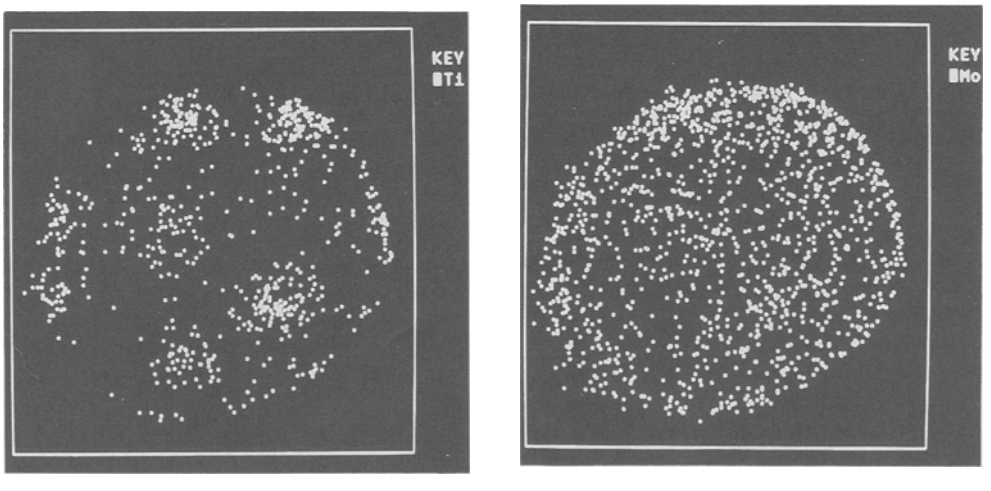

(*b*)

Fig. 9—POSAP images of C-300 maraging steel aged at 510 °C, showing the distribution of Ti and Mo. Each dot represents one atom. Data were collected from a depth of 1 to 2 nm. Distance across the images is ≈25 nm. (*a*) Aged for 240 s; (*b*) aged for 460 s. (Reproduced courtesy of Pergamon Press.)

Table IV. Composition of Particles for Short Aging Times as Determined by POSAP

Aging Time (s)	Ti	Mo*
240	8 ± 2 (6 to 13)	2 ± 2 (0 to 8)
460	14 ± 4 (10 to 22)	4 ± 1 (2 to 5)

*In this table, the Mo concentrations were determined by using Mo^{2+} only. The approximate real Mo concentration may be obtained by multiplying the apparent concentration shown by a factor of 1.5 (this factor was deduced from POSAP data for as-quenched material).

and coarsening processes of these precipitates. The diameter of the Ti particles estimated from the POSAP images is ≈5 nm in the case of the 460-second aged material. The number density of the clusters was estimated to be of the order of 10^{23} m^{-3} both from POSAP and FIM100 AP analysis. The crystal structure of the particles cannot readily be determined from FIM observations. However, the continuity of image rings in the sequence of FIM micrographs shown in Figure 7 indicates a high degree of coherency between the particles and the matrix in the early stages of aging.

D. *APFIM Study II—Near Peak-Hardness Aging Reactions*

1. *Precipitates*

Figure 10 shows a field-ion micrograph of the steel after aging for 2 hours at 510 °C, *i.e.*, near peak hardness. A large number of brightly imaged precipitate particles can be seen throughout the field of view. These precipitates are substantially larger in size than the probe hole aperture (which can be seen as a small black area at the center of the image), and consequently, accurate AP analyses of individual particles can be carried out.

From the analyzed compositions (Table V), it is evident that two distinct families of precipitates have formed at this stage of aging, corresponding to Fe_7Mo_6 (μ phase) and Ni_3Ti, respectively. (For a more detailed discussion of the identification of the Fe-Mo phase, see Part IV of this series.[26]) The Fe_7Mo_6 μ phase has some of its Fe substituted by Ni and a small amount by Co. The presence of Si in μ phase is reasonable if one considers the affinity between Mo and Si in the steel. The Ni_3Ti-type precipitate has some of its Ni substituted by Fe and a small amount by Co and has some Mo in solid solution probably due to the interaction between Ni and Mo. The presence of Al in this precipitate is due to the chemical affinity between Ni and Al in the material. Cobalt contents in both families of precipitates are lower by a factor of 2 to 4 than the bulk composition.

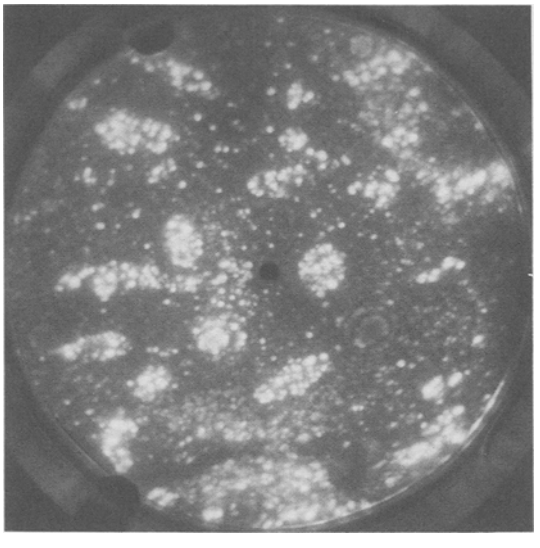

Fig. 10—Field-ion micrograph of a precipitated area in a C-300 maraging steel sample aged at 510 °C for 2 h. Precipitates are imaged brighter than martensite matrix. Distance across the image is ≈125 nm.

The compositions of the Ni_3Ti precipitates vary widely (Table Vb). The general trends are that Ni content increases with increasing aging time, while Mo and Fe contents decrease.

The coexistence of these two kinds of precipitates adjacent to each other was also observed (Figure 11). It is believed that Ni_3Ti forms first, because of its smaller lattice misfit with the martensite matrix, and the more stable μ phase forms later. The supply of Mo from the Ni_3Ti and relatively unstable state near the interface would make the adjacent area the ideal place for μ phase to nucleate. Such a process seems to happen most strongly after 2 hours of aging, which explains why the chemical analyses of Ni_3Ti-type precipitates in specimens aged for this time vary widely. Composition analysis showed instances of Mo enrichment at the interface between Ni_3Ti and the matrix, which might represent the very initial stage of formation of some μ-phase precipitates.

Field evaporation sequences revealed that the Ni_3Ti precipitates, which image less brightly than Fe_7Mo_6, are rod-shaped (rod diameter, 5 to 10 nm; length, 15 to 30 nm). The Fe_7Mo_6 precipitates are mostly spheroidal (diameter, 10 to 30 nm) when the aging time is not very long and become difficult to assess in detail by FIM techniques when they grow very large after long-term aging.

From the apparent continuity between atomic planes of precipitates and matrix, the precipitates appear to retain some degree of coherency with the martensite matrix. This is in agreement with previous authors.[2,27] Ladder diagram analysis shows that there is an atomically sharp interface between the precipitates and the martensite matrix.[14] Segregation of impurities (Si, C, Cr) was sometimes found at the interfaces between Ni_3Ti precipitates and the martensite matrix. The equivalent interfaces between μ-phase precipitates and the matrix appeared to be free of segregation effects.

It should be noted that apart from the fine isolated precipitates, there are much less frequent larger platelike ones (Figure 12). These precipitates appear to have formed principally at martensite lath boundaries, though the possibility of some being at prior austenite grain boundaries cannot be completely ruled out. Some regions of the platelike precipitates in Figure 12 were found to be Mo-rich, but others were Ti-rich. Quantitative composition analysis for these precipitates is not available due to the very narrow width of the precipitation band. Boundary precipitation has been suggested by the early work of Spitzig *et al.*[28] Magnee *et al.* have also mentioned that Mo preferred to segregate at lath martensite

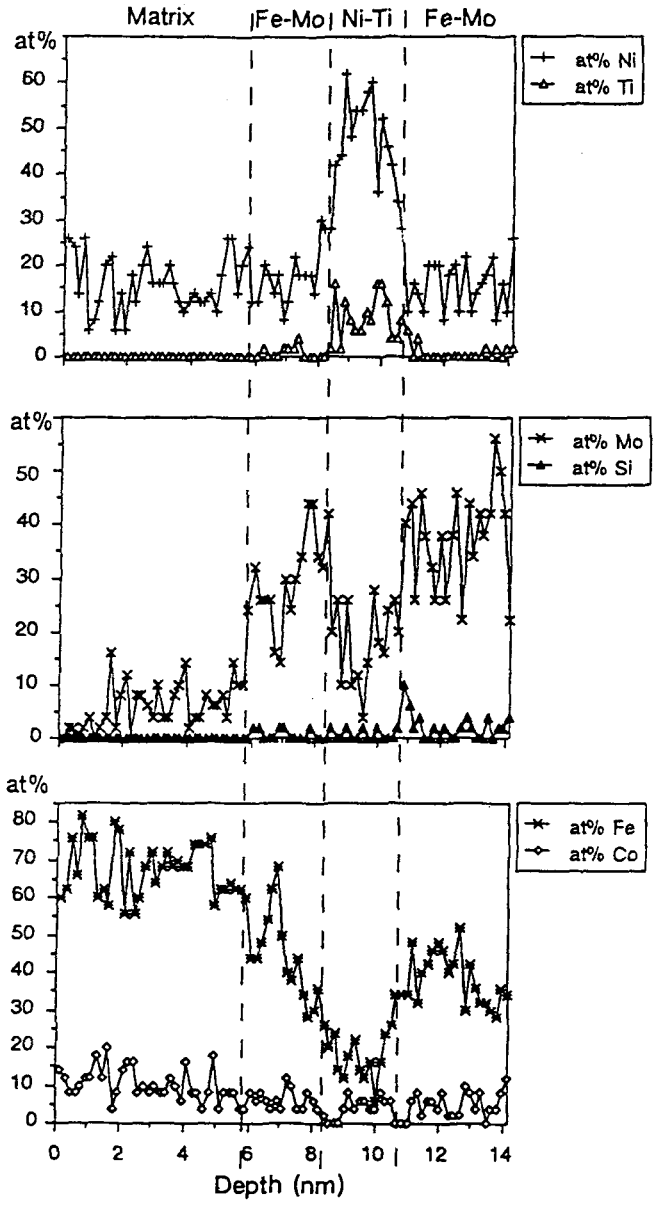

Fig. 11—Composition profiles of the C-300 maraging steel aged for 4 h at 510 °C, across a μ-Ni_3Ti-μ region. Note the depletion of Co at the interfaces between two kinds of precipitates. The mechanism for such an effect is not clear.

boundaries,[3] and instances of single atomic layer decoration of Mo were observed in the FIM during the present work, which might be the very initial stage of boundary precipitation.

2. *α matrix and reverted austenite*

The matrix composition has also been measured after various aging treatments (Table VI). The measured matrix Mo solute content is useful for comparing the behavior of different steels, which will be further discussed in Part IV.[26] There is a progressive depletion of solute Mo. Titanium depletes very early on during aging. Nickel content rises with increasing aging time, since the amount of Mo-enriched Ni_3Ti decreases as Mo moves to the μ phase. The matrix Co level is generally above the bulk composition of the steel. This reflects the preferential partitioning of Co to the matrix during the formation of the Ni_3Ti and Fe_7Mo_6 precipitate phases. The amount of Ti left in the matrix is very small and nearly undetectable.

Austenite reversion after aging for $\geq$4 hours has been detected and analyzed (Table VII). With increasing aging time, the austenite Ni and Ti contents decrease toward the equilibrium concentrations (see Section IV). This suggests the possibility of austenite nucleation on sites near metastable Ni_3Ti particles.

E. *APFIM Study III—Overaging*

Figure 13 shows a field-ion micrograph taken from a sample aged for 128 hours at 510 °C. The FIM observations and AP composition analysis of this material showed the existence of four phases: α matrix, austenite, and the two families of intermetallics (Ni_3Ti and Fe_7Mo_6). The compositions of these four phases are shown in Table VIII. The precipitates can be either embedded in the α matrix or adjacent to austenite. It should be noted that the matrix Ni content drops to about 9 pct after 128 hours of aging. This is clearly linked to the more extensive formation of reverted austenite (which acts as a sink for this element). The Ni level in austenite essentially agrees with a previous study by Schmidt.[29]

Using the mass balance of these four phases and four alloying elements (Ni, Co, Mo, Ti) and assuming the density difference to be negligible, the volume percentages of these phases can be obtained (the last row of Table VIII). The results fit quite well for the mass balance of Fe, confirming the validity of the calculation. The volume percentage of austenite is lower than the predicted value, and not all of the alloying elements are thoroughly redistributed. The Ni_3Ti phase, thermochemically calculated to be a nonequilibrium phase (see Section IV), is still present in the aged structure. This indicates that even after aging for 128 hours, the alloy is still some way removed from its final equilibrium state.

IV. THERMOCHEMICAL CALCULATIONS

The Thermo-Calc software uses a data bank of assessed thermochemical data and models for alloys phases.[30] With the Thermo-Calc Alloy (Steel) Data Base in this software, the equilibrium state of the steel in 510 °C has been calculated. Possible equilibrium phases relevant to this maraging steel system in the data base and entered into calculations include body-centered cubic (bcc) matrix, face-centered cubic (fcc) austenite, Si diamond cubic, FeSi, Fe_2Si, Fe_5Si_3, $FeSi_2$-H, $FeSi_2$-L, Fe_2Mo Laves phase, Ni_3Mo γ, Ni_4Mo β, NiMo δ, Fe_7Mo_6 μ, R, and FeMo σ. One drawback of the Thermo-Calc Alloy Data Base is that the Ni_3Ti phase is not included. From the literature and current experimental results, this phase is very important in the present maraging steel systems. In the other available data base (Kaufman) in the Thermo-Calc software, Ni_3Ti is included but Fe_2Mo phase is not. Calculations were performed in the Kaufman data base and the Ni_3Ti phase was not stable, which is in agreement with many previous studies suggesting that Ni_3Ti is a metastable precipitate in maraging steels. The calculation results from the Thermo-Calc Alloy Data Base

Table V. Compositions of the Two Kinds of Precipitates in 510 °C Aged C-300 Maraging Steel Measured by FIM100 Atom Probe

(a) Fe_7Mo_6 Type

Aging Time (h)	Mo	Fe	Ni	Co	Si
0.5	45.6 ± 8.1	30.7 ± 3.2	12.1 ± 3.0	3.0 ± 1.4	7.4 ± 1.8
1	41.5 ± 2.8	39.5 ± 3.5	14.5 ± 2.5	2.0 ± 1.0	1.8 ± 1.1
2	43.7 ± 5.5	34.1 ± 3.7	15.9 ± 5.2	3.0 ± 1.0	2.1 ± 1.4
4	39.2 ± 5.8	36.9 ± 5.3	15.8 ± 2.6	4.0 ± 0.5	4.0 ± 1.5
8	43.5 ± 4.7	37.8 ± 3.5	11.3 ± 1.9	4.3 ± 0.8	2.0 ± 1.0

(b) Ni_3Ti Type

Aging Time (h)	Ni	Fe	Co	Ti	Mo	Al
0.5	43.9 ± 3.7	18.4 ± 2.9	3.6 ± 1.3	19.9 ± 2.8	13.0 ± 3.4	1.0 ± 1.0
1	55.8 ± 3.3	12.4 ± 4.6	3.0 ± 1.2	13.5 ± 3.4	14.1 ± 1.6	1.1 ± 0.2
2*	40.5 ± 9.0	23.5 ± 8.9	4.1 ± 3.3	20.0 ± 8.9	10.5 ± 7.6	1.7 ± 0.5
4	54.7 ± 2.4	13.6 ± 1.2	3.5 ± 1.9	12.6 ± 1.1	14.9 ± 1.5	0.4 ± 0.4
8	65.4 ± 1.8	7.8 ± 3.0	1.1 ± 0.5	19.9 ± 3.3	4.2 ± 2.0	1.4 ± 1.0

*This excludes one precipitate for which the analysis was $Ni_{57\pm4}Fe_{14\pm3}Co_{6\pm2}Ti_{3\pm1}Mo_{20\pm3}Al_{1\pm1}$. It is possible that this was an isolated ω-phase particle of the type found more commonly in Ti-free model alloys (see Part III[32]).

Table VI. Composition of Matrix in 510 °C Aged C-300 Maraging Steel Measured by FIM100 Atom Probe

Aging Time (h)	Fe	Ni	Co	Mo	Ti
0.5	75.5 ± 6.3	12.0 ± 3.3	9.2 ± 3.6	1.4 ± 0.5	0.1 ± 0.1
1	75.2 ± 2.4	13.0 ± 1.9	10.3 ± 1.4	1.2 ± 0.5	0.1 ± 0.1
2	77.5 ± 4.9	12.6 ± 3.4	8.6 ± 2.3	1.1 ± 0.6	<0.1
4	74.3 ± 0.4	14.3 ± 0.3	10.2 ± 0.3	1.0 ± 0.1	0.04 ± 0.02
8	73.6 ± 1.2	16.3 ± 1.0	9.1 ± 0.8	0.6 ± 0.2	0.08 ± 0.08

Table VII. Composition of Reverted Austenite in 510 °C Aged C-300 Maraging Steel Measured by FIM 100 Atom Probe

Aging Time (h)	Fe	Ni	Co	Mo	Ti	Al
4	38.3 ± 3.3	49.0 ± 3.4	6.3 ± 1.6	3.2 ± 1.2	2.7 ± 1.1	0.5 ± 0.5
8	54.0 ± 0.8	37.3 ± 0.8	5.1 ± 0.4	2.9 ± 0.3	0.4 ± 0.1	0.3 ± 0.1

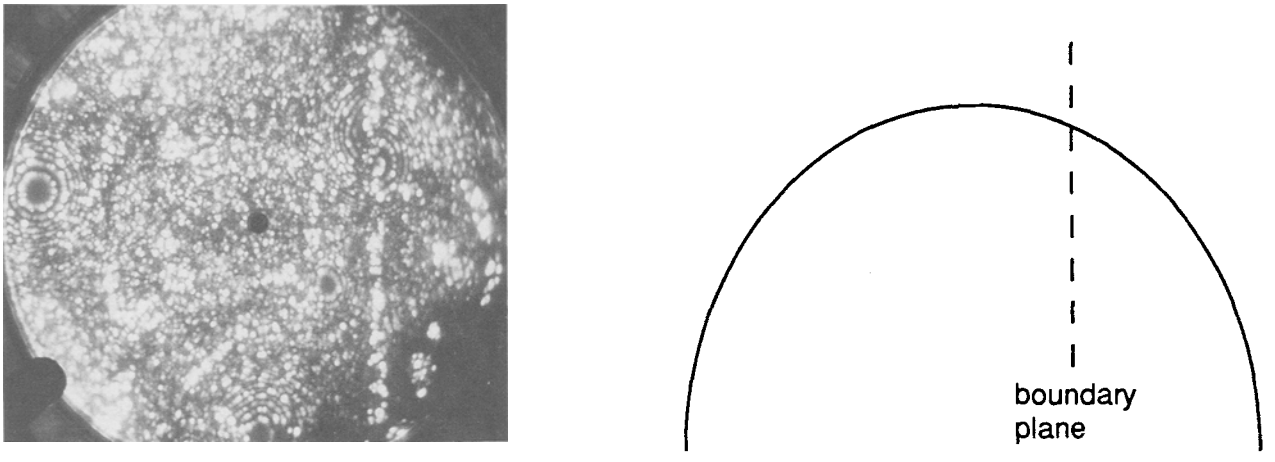

(*a*) (*b*)

Fig. 12—Field-ion micrograph (*a*) with accompanying sketch of tip orientation (*b*) showing relatively large platelike precipitates in C-300 maraging steel aged at 510 °C for 2 h. Distance across the image is ≈140 nm. The discontinuity of the rings across the precipitates suggests that these lie on a lath boundary.

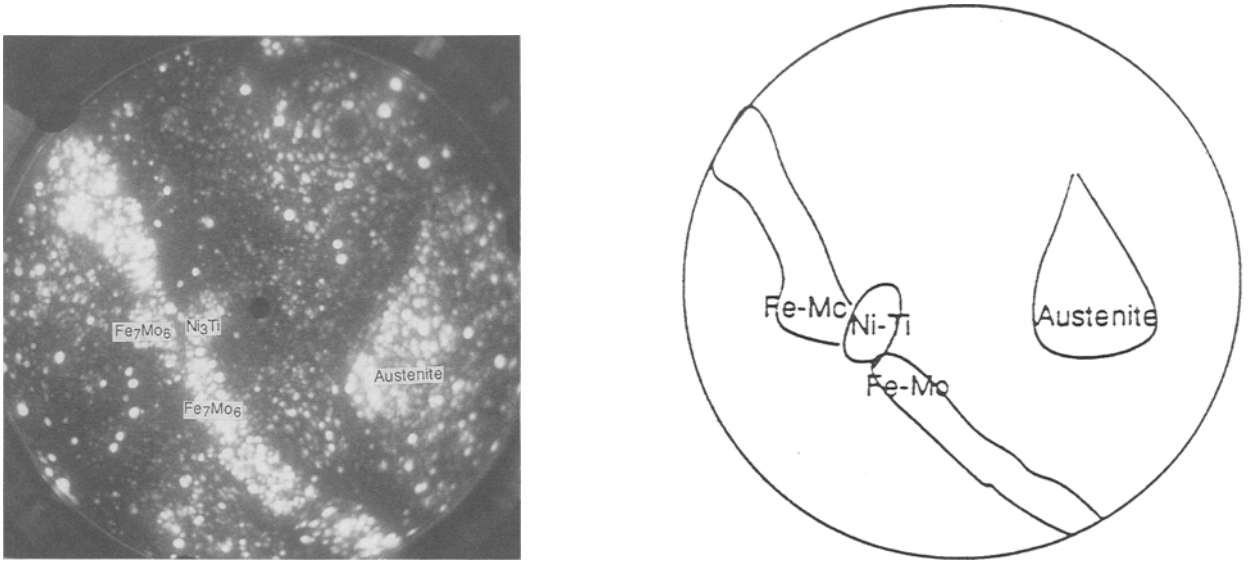

(*a*) (*b*)

Fig. 13—(*a*) Field-ion micrograph of a C-300 maraging steel sample aged at 510 °C for 128 h. Distance across the image is ≈120 nm. The phase identifications by AP are shown. (*b*) Key to (a).

Table VIII. Phase Compositions and Their Respective Volume Percentages for C-300 Maraging Steel Aged at 510 °C for 128 Hours: Atom-Probe Result

Phase	Fe	Ni	Co	Mo	Ti	Al	Si	Volume Percent
α matrix	77.9 ± 0.6	9.3 ± 0.4	12.4 ± 0.5	0.4 ± 0.1	<0.1	<0.1	<0.1	≈67
Austenite	53.5 ± 1.9	39.2 ± 2.4	3.5 ± 0.7	2.7 ± 0.9	0.3 ± 0.1	0.3 ± 0.1	<0.1	≈26
Fe_7Mo_6	39.3 ± 4.1	13.1 ± 2.4	3.8 ± 2.0	41.2 ± 2.5	<0.1	<0.1	1.5 ± 1.0	≈ 4
Ni_3Ti	3.5 ± 1.1	70.4 ± 1.3	2.0 ± 0.2	3.9 ± 0.2	17.9 ± 0.8	2.2 ± 0.5	<0.1	≈ 3

are demonstrated here. This is useful in comparing the stabilities of Fe_2Mo and Fe_7Mo_6.

The calculated equilibrium state consists of bcc α matrix, austenite, and Fe_7Mo_6 μ phase for the steel. Table IX gives the equilibrium composition of the three phases in the steel at 510 °C. The equilibrium Mo content in austenite is calculated to be higher than that in the α matrix. This at first seems to be contrary to the role of Mo in the stabilization of ferrite, as suggested by the Fe-Mo phase diagram.[31] But considering the affinity between Ni and Mo, the result is not unreasonable for this particular alloy system. Furthermore, the thermochemical calculation result for austenite composition agrees very well with the measured austenite composition (compare Tables VIII and IX). Table X gives the calculated driving forces of different phases in the steel at 510 °C, showing that the Fe_7Mo_6 μ phase has the largest driving force for precipitation.

V. CONCLUSIONS

No detectable clustering exists in the as-quenched state in the Co-containing C-300 maraging steel. Two families of intermetallic phases have been found to contribute to age hardening. The decomposition seems to start with the formation of small Mo-enriched Ni_3Ti particles at very short aging times. The Fe_7Mo_6 phase forms at a later stage of aging. Some of the Fe_7Mo_6 precipitates may nucleate at the boundaries of the Ni_3Ti phase or martensite lath boundaries. The observation of the Fe_7Mo_6 μ phase is supported by thermochemical calculations. Austenite

Table IX. Equilibrium Phase Compositions and Their Respective Volume Percentages for C-300 Maraging Steel at 510 °C: Thermo-Calc Thermochemical Calculation Result

Phase	Fe	Ni	Co	Mo	Ti	Al	Si	Volume Percent
α matrix	79.8	4.1	13.6	0.7	1.3	0.1	0.4	53.7
Austenite	56.6	38.3	3.6	1.1	*	0.4	0.0	41.6
Fe_7Mo_6	55.0	0.6	0.0	44.4	*	*	*	4.7

*Element not included as a phase constituent in the data base (Table V).

Table X. Driving Forces for Precipitation of Phases in C-300 Maraging Steel System at 510 °C: Thermo-Calc Thermochemical Calculation Result

Phase	Phase Constituent Included	State*	Driving Force $\Delta G/RT$
Bcc matrix	Fe, Ni, Co, Mo, Ti, Al, Si	entered	0
Fcc austenite	Fe, Ni, Co, Mo, Al, Si	entered	0
FeSi	Fe, Si	dormant	− 4.4
Fe_2Si	Fe, Si	dormant	− 2.4
Fe_5Si_3	Fe, Si	dormant	− 2.8
$FeSi_2$-H	Fe, Si	dormant	−10.1
$FeSi_2$-L	Fe, Si	dormant	− 8.5
Fe_2Mo Laves	Fe, Mo	dormant	1.0
Ni_3Mo γ	Ni, Mo	dormant	− 3.6
Ni_4Mo β	Ni, Mo	dormant	− 5.1
NiMo δ	Ni, Mo	dormant	−14.4
Fe_7Mo_6 μ	Fe, Mo, Ni, Co	dormant	6.8
R	Fe, Mo, Co	dormant	4.5
FeMo σ	Fe, Mo, Ni, Co	dormant	3.5

*A dormant phase is included in the calculation but not allowed to transform. It is used to calculate the driving force of the phase transformation. A negative driving force means that the phase has no tendency to form. The value of a positive driving force is proportional to the tendency to form. When a phase is entered in the calculation and remains stable, its driving force will be 0.

reversion begins to occur after aging for 4 hours at 510 °C.

ACKNOWLEDGMENTS

The authors would like to thank Dr. H.-O. Andrén and the late Dr. M.G. Hetherington for discussions, Mr. T.J. Godfrey for technical assistance, Professor Sir Peter Hirsch for the provision of laboratory facilities, and Dr. D.M. Vanderwalker of the United States Army Materials Technology Laboratory for supplying the original samples. The Oxford AP facilities are partly funded by the Science and Engineering Research Council (UK) under Grant No. GR/F/06111. The authors are also grateful to The British Council (WS), The Royal Society, and Wolfson College, Oxford (AC), for financial support.

REFERENCES

1. S. Floreen: *Metall. Rev.*, 1968, vol. 13, pp. 115-28.
2. R.F. Decker and S. Floreen: in *Maraging Steels: Recent Developments and Applications*, R.K. Wilson, ed., TMS-AIME, Warrendale, PA, 1988, pp. 1-38.
3. A. Magnee, J.M. Drapier, J. Dumont, D. Coutsourdis, and L. Habraken: *Cobalt-containing High-strength Steels: A Critical Review of the Physical Metallurgy of Cobalt-containing High-strength Steels, and a Survey of Their Processing, Properties and Uses*, Centre D'Information Du Cobalt, Brussels, 1974, pp. 50-123.
4. K. Ogawa, M. Fukamachi, and Y. Kawabe: *Nippon Kinzoku Gakkaishi*, 1983, vol. 47, pp. 863-67.
5. A.F. Edneral, V.B. Dmitriev, A.N. Kudryavtsev, and V.V. Rusanenko: *Dokl. Akad. Nauk SSSR*, 1984, vol. 278, pp. 612-15.
6. A.N. Kudryavtsev and A.F. Edneral: *Dokl. Akad. Nauk SSSR*, 1981, vol. 261, pp. 611-15.
7. M. Fukamachi, Y. Kawabe, K. Nadazawa, and S. Muniki: *Nippon Kinzoku Gakkaishi*, 1983, vol. 47, pp. 237-42.
8. J.R. Mihalisin and C.G. Bieber: *J. Met.*, 1966, vol. 18, pp. 1033-36.
9. V.K. Vasudevan, S.J. Kim, and C.M. Wayman: in *Maraging Steels: Recent Development and Applications*, R.K. Wilson, ed., TMS-AIME, Warrendale, PA, 1988, pp. 283-94.
10. V.K. Vasudevan, S.J. Kim, and C.M. Wayman: *Metall. Trans. A*, 1990, vol. 21A, pp. 2655-68.
11. M.K. Miller and G.D.W. Smith: *Atom Probe Microanalysis: Principles and Applications to Materials Problems*, MRS, Pittsburgh, PA, 1989.
12. A.F. Edneral, V.I. Kirienko, and L.P. Potapov: *Dokl. Akad. Nauk SSSR*, 1973, vol. 213, pp. 567-68.
13. V.P. Khlyntsev, A.N. Kudryavtsev, L.P. Potapov, and V.I. Kirienko: *Fiz. Met. Metalloved.*, 1979, vol. 47, pp. 815-20.
14. A. Cerezo, C.R.M. Grovenor, M.G. Hetherington, W. Sha, B.A. Shollock, and G.D.W. Smith: *Mater. Charact.*, 1990, vol. 25, pp. 143-56.
15. W. Sha, A. Cerezo, and G.D.W. Smith: *J. Phys. Colloq.*, 1989, vol. 50-C8, pp. 407-12.
16. W. Sha, A. Cerezo, and G.D.W. Smith: *Surf. Sci.*, 1991, vol. 246, pp. 286-92.
17. W. Sha, G.D.W. Smith, and A. Cerezo: *Surf. Sci.*, 1992, vol. 266, pp. 378-84.
18. W. Sha, A. Cerezo, and G.D.W. Smith: *Scripta Metall. Mater.*, 1992, vol. 26, pp. 517-28.
19. A. Gemperle, J. Gemperlová, W. Sha, and G.D.W. Smith: *Mater. Sci. Technol.*, 1992, vol. 8, pp. 546-54.
20. D.M. Vanderwalker: in *Maraging Steels: Recent Development and Applications*, R.K. Wilson, ed., TMS-AIME, Warrendale, PA, 1988, pp. 255-68.
21. D.M. Vanderwalker: *Metall. Trans. A*, 1987, vol. 18A, pp. 1191-14.
22. C. Servant, G. Maeder, and G. Cizeron: *Metall. Trans. A*, 1975, vol. 6A, pp. 981-90.
23. C.F. Hickey, Jr., D.W. Dix, and D. Kagan: *Mechanical Property Characterization of VascoMax T-300*, United States Army Materials Technology Laboratory Report, MTL TR 89–81, p. 5.
24. D.T. Peters: *Trans. ASM, Trans. Q.*, 1968, vol. 61, pp. 62-74.
25. J.M. Papazian: *J. Microsc.*, 1972, vol. 95, p. 429.
26. W. Sha, A. Cerezo, and G.D.W. Smith: *Metall. Trans. A*, 1993, vol. 24A, pp. 1251-56.
27. J.B. Lecomte, C. Servant, and G. Cizeron: *J. Mater. Sci.*, 1985, vol. 20, pp. 3339-52.
28. W.A. Spitzig, J.M. Chilton, and C.J. Barton: *Trans. ASM*, 1968, vol. 61, pp. 635-39.
29. M.L. Schmidt: in *Maraging Steels: Recent Developments and Applications*, R.K. Wilson, ed., TMS-AIME, Warrendale, PA, 1988, pp. 213-36.
30. B. Sundman, B. Jansson, and J.-O. Andersson: *CALPHAD*, 1985, vol. 9, p. 150.
31. *Binary Phase Diagrams*, 2nd ed., T.B. Massalski, ed., ASM, Metals Park, OH, 1990.
32. W. Sha, A. Cerezo, and G.D.W. Smith: *Metall. Trans. A*, 1993, vol. 24A, pp. 1241-49.